Journal of Energy Storage 21 (2019) 321–327

Contents lists available at ScienceDirect

Journal of Energy Storage

journal homepage: www.elsevier.com/locate/est

# Understanding the redox reaction mechanism of vanadium electrolytes in all-vanadium redox flow batteries

Chanyong Choi[a,b], Hyungjun Noh[a,b], Soohyun Kim[a,b], Riyul Kim[a,b], Juhyuk Lee[a,b], Jiyun Heo[a,b], Hee-Tak Kim[a,b,*]

[a] Department of Chemical and Biomolecular Engineering, Korea Advanced Institute of Science and Technology, 291 Daehak-ro, Yuseong-gu, Daejeon, 305-701, Republic of Korea

[b] Advanced Battery Center, KAIST Institute for the NanoCentury, Korea Advanced Institute of Science and Technology, 335 Gwahangno, Yuseong-gu, Daejeon, 34141, Republic of Korea

ARTICLE INFO

*Keywords:*
Vanadium redox flow battery
Impedance analysis
Symmetric cell
Inner sphere mechanism
Outer sphere mechanism

ABSTRACT

Vanadium redox flow batteries (VRFBs) have been highlighted for use in energy storage systems. In spite of the many studies on the redox reaction of vanadium ions, the mechanisms for positive and negative electrode reaction are under debate. In this work, we conduct an impedance analysis for positive and negative symmetric cells with untreated and heat-treated carbon felt (CF) electrodes to identify the reaction mechanisms. The negative electrode reaction ($V^{2+}/V^{3+}$) is highly dependent on the heat treatment and reaction temperature, which is a feature of an inner-sphere mechanism, whereas the positive electrode reaction ($VO_2^+/VO^{2+}$) reaction is rather insensitive to the heat treatment and reaction temperature, suggesting an outer-sphere mechanism. An atomistic molecular dynamics simulation suggests that the different mechanisms are quite feasible considering the difference in the structure of the hydration shell for the vanadium ions. The deeper understanding of the reaction mechanism and its influence on cell performance will be helpful to advance VRFBs.

## 1. Introduction

The need for large-scale energy storage systems (ESSs), which can store electric energy and release it on demand, is continually increasing due to increased energy consumption and the expanded use of renewable [1]. Safety and reliability are the primary requisites for a large-scale ESS, and, in this regard, VRFBs, which feature high chemical stability, long cycle life, and flexible modular design, have attracted interest for the past several years [2–4]. In addition, to achieve high energy efficiency, numerous research groups have sought to improve the electrochemical performance of VRFBs.

The redox reactions of $VO_2^+/VO^{2+}$ at the positive electrode (PE) and that of $V^{2+}/V^{3+}$ at the negative electrode (NE) are described in Eqs. (1) and (2), respectively.

$$\text{Positive:} \quad VO_2^+ + 2H^+ + e^- \rightarrow VO^{2+} + H_2O \tag{1}$$

$$\text{Negative:} \quad V^{2+} \rightarrow V^{3+} + e^- \tag{2}$$

As an electrode for the positive and negative reaction, CFs with surface functional groups (−OH) are conventionally employed due to their high electronic conductivity, high porosity, and high wettability in aqueous vanadium electrolytes. A sound understanding of the reaction kinetics and mechanism for these redox reactions is important for advanced electrode and electrolyte material design and optimizing operation conditions. M. Kazacos and coworkers proposed a mechanism for these reactions [3,5,6]; the key feature of which is that the −OH functional group serves as an adsorption site of vanadium ions, facilitating electron transfer for both reactions and oxygen transfer for both the positive and negative reaction. They also suggested that the positive reaction is slower than the negative reaction due to the presence of a slower oxygen transfer step. Recently, Kazacos group [7,8] proposed revised views; the redox reaction of V(IV)/V(V) and V(II)/V(III) are related to the specific surface area and degree of electrolyte wetting. The increase of electrode surface area due to the degradation by V(V) solution and consequent increase of the redox activity of positive electrode were emphasized. Z. Liang group reported the redox reaction of vanadium ions on Vulcan carbon [9] and nitrogen-doped carbon [10] via in-depth electrochemical analysis. They claimed that the redox reaction of $V^{3+}/V^{2+}$ is determined by diffusion process with outer-sphere mechanism. On the contrary, the kinetic of $VO^{2+}/VO_2^+$ is much lower

* Corresponding author at: Department of Chemical and Biomolecular Engineering, Korea Advanced Institute of Science and Technology, 291 Daehak-ro, Yuseong-gu, Daejeon, 305-701, Republic of Korea.
*E-mail address:* heetak.kim@kaist.ac.kr (H.-T. Kim).

https://doi.org/10.1016/j.est.2018.11.002
Received 28 August 2018; Received in revised form 2 November 2018; Accepted 2 November 2018
Available online 13 December 2018
2352-152X/ 

than that of $V^{2+}/V^{3+}$ due to the proceding adsorption process. Some works on a half-cell analysis of the PE and NE reactions support this mechanism [11–14].

However, some groups including our group [15–17] recently reported the monitoring of PE and NE polarization by using a dynamic hydrogen electrode for a full cell and discovered that the NE polarization is much larger than the PE polarization, which does not agree with the suggested mechanism. In addition, based on a rate constant analysis with a varying degree of surface functionalization, the Stimming group suggested that the PE reaction follows outer-sphere electron transfer during vanadium ion-electrode collision process, whereas the NE reaction follows inner-sphere electron transfer that accompanies adsorption of the reactant and consequent electron transfer between the electrode and adsorbed reactant [18]. M. Zago group evaluated the electrochemical performance by installing through-plate reference electrodes at inlet and outlet of electrolyte tanks [19]. They reported the potential loss at the negative electrode dominated at inlet of the cell below 0.4 $Acm^{-2}$ current densities. It indicated that overpotential at negative electrode is higher than that of positive due to slow kinetics. As outlined above, the mechanism for the redox reactions in a VRFB full cell remains unclear due to the lack of sufficient electrochemical analysis. In fact, there is an debate on which electrode reaction is slower between positive and negative electrode reaction. The conflicting results of the previous studies [12–15,17,18,20–23] are summarized in Table S1.

Nonetheless, the inconsistency in the reaction mechanism could be partly due to differences in the analysis system. Many previous works on electrochemical analysis of VRFB reactions were conducted in a half-cell configuration or a static mode with carbon paper or disc electrode [12,16,24–26]. The surface structures and interfacial environments of the working electrode for these analyses can vary due to the difference in carbon material, cell configuration, and flowing conditions. In this light, to clearly identify the reaction mechanism, it is necessary to investigate the redox reactions for the conventionally adopted CF electrode in a full cell configuration under practical operating conditions.

Here, with the aim of elucidating the mechanism of PE and NE reactions in a VRFB, we conducted an impedance analysis for a symmetric cell where the configuration and materials are identical to those of a full cell. A positive ($VO_2^+/VO^{2+}$) or negative ($V^{2+}/V^{3+}$) electrolyte was circulated through both compartments of the symmetric cell, which is denoted as a positive single cell and a negative single cell, respectively, and AC impedances of the symmetric cells were monitored. The symmetric cell analysis comprehensively dictates the PE and NE reaction in a full cell without any perturbation from vanadium ion crossover or potential drift of the internal reference electrode, which is the major incentive of the methodology suggested in this work. Also, we compared untreated CF (U-CF) and heat-treated CF (T-CF) for the PE and NE reaction to identify whether the adsorption of vanadium ions is a critical step for the electron transfer.

## 2. Experimental section

### 2.1. Material preparation

CF (NF-1311, Jiuhua Hi-Tech Co., Ltd., China) was purchased and treated at 520 °C for 9 h in an air condition to generate oxygen functional groups onto the surface of the CF. Electrolyte was prepared by dissolving 1.5 M $VOSO_4 \cdot nH_2O$ (99%, Prudent co., n = 3.5) in 3 M sulfuric acid solution (95%, Aldrich). $VO_2^+$ (V(V)) and $V^{2+}$ (V(II)) electrolyte were electrochemically synthesized from the V(IV) electrolyte. Electrolyte with SOC 50 was prepared by discharging 50% capacity from the fully charged electrolyte. The OCV of electrolyte with SOC 50 solution was 1.4 ± 0.005 V. NRE 115 membrane was purchased from Dupont.

### 2.2. Electrochemical characterization

A 20 $cm^2$ sized (5 cm × 4 cm) VRFB single cell that consists of end plates, gold current collectors, bipolar plates, gasket, electrodes and membranes was constructed. U-CF or T-CF was used for PE or NE. NRE 115 membrane was used as a separator. The single cell was used for the symmetric cell and full cell analysis. All the vanadium electrolytes were circulated by pumps (Masterflex). The flow rate was 40 mL $min^{-1}$ for charging. Charge and discharge of the VRFB were conducted at room temperature (25 ± 2 °C) by using a battery cycler (WBCS 3000, Won-A tech).

For electrochemical impedance spectroscopy, a potentiostat (a Biologic VSP) was used. AC impedances were measured for the symmetric cells in a 2-electrode mode, in a frequency range from 100 kHz to 0.1 kHz, and with a potential amplitude of 20 mV. The OCV of positive/negative symmetric cell were strictly maintained below 1 mV. To measure temperature-dependant impedances, a full cell system including the electrolyte reserviors, pump and symmetric cell were installed in a temperature-controlled oven and equilbrated at a designated temperature before the impedance measurement. A modified Randles circuit model featuring a parallel combination of constant phase element and resistance was used to determine the charge transfer resistance of the electrodes. The observed charge transfer resistances from the symmetric cells were divided by two to express that of a single electrode, because two identical electrodes are connected in series for the symmetric cell.

### 2.3. Material characterization

The C1s and O1s atomic content of U-CF or T-CF were measured by using X-ray photoelectron spectroscopy (Sigma Probe, Thermo VG Scientific) with Al Ka as the X-ray source. The binding energy was calibrated against the C 1s peak (C═C, $sp^2$ hybridization) at 284.6 eV. Contact angle measurement was performed with a Pheonix 300(SEO).

### 2.4. Molecular dynamics (MD) simulations

MD simulations for the vanadium ions in sulfuric acid solution were performed with Materials Studio (Biovia Inc.) software. These were done with a fully atomistic model of the vanadium ($V^{2+}$, $V^{3+}$, $VO^{2+}$ and $VO_2^+$), $H_2O$, $SO_4^{2-}$, and proton. Before MD simulation, Each molecule was geometry optimized by the built-in Dmol module. The Perdew-Burke-Ernzerhof generalized gradient approximation (GGA-PBE) was selected as the exchange-correlation functional. We then constructed four different vanadium ions with $H_2SO_4$ lattice models consisting of 15 $V^{2+}$, $V^{3+}$, $VO^{2+}$, and $VO_2^+$, 45 $SO_4^{2-}$, 60 protons, and 555 $H_2O$ molecules using the built-in Amorphous Cell module. The formed amorphous cell was assigned by using the Forcite module and forcefield COMPASS II. The MD simulations were run for 1 ns at 298 K in NPT ensemble (P = 1 atm). The simulation runs were then conducted for 1 ns at 298 K in NVT ensemble. The Ewald summation method with an accuracy of 0.001 $kcalmol^{-1}$ and the atom based summation were selected for calculating the electrostatic interactions and Van der Waals interactions, respectively. During NPT and NVT ensemble, a NHL algorithm with a 0.01 Q ratio and 1.0 ps decay constant was used to control the temperature and pressure.

## 3. Results and discussion

To investigate the effect of the oxygen functional group on the surface property of the CF, water drop contact angle tests were conducted for U-CF and T-CF. As shown in Fig. 1(a) and (b), the contact angle measured from the U-CF is 130°, while that of T-CF cannot be measured due to being absorbed water drops in T-CF. This shows that T-CF became hydrophilic after the heat treatment. The oxygen functional group generated by the heat-treatment was confirmed by a C1s

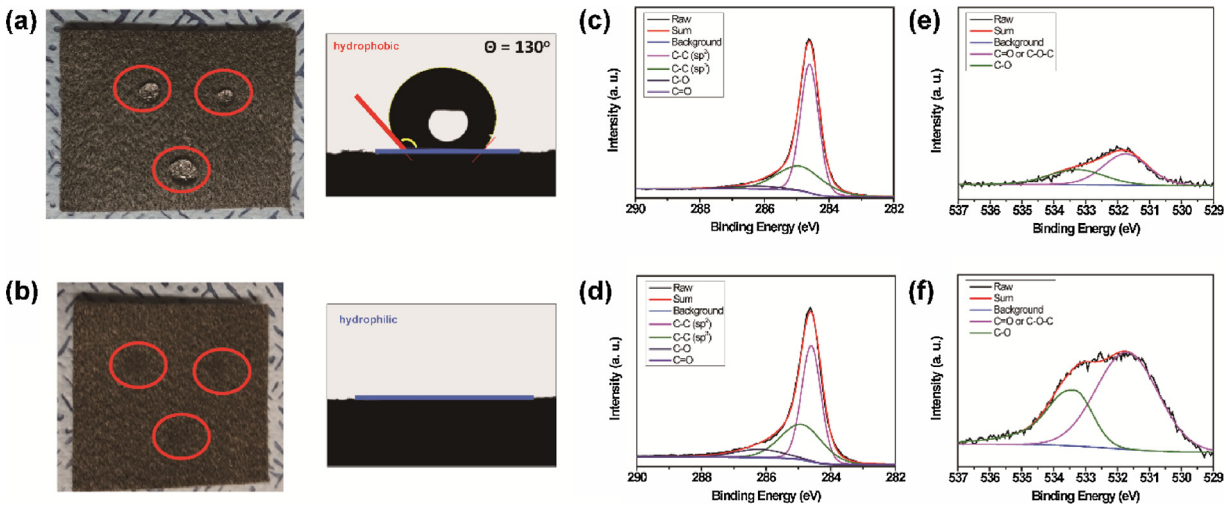


**Fig. 1.** Characterization of the U-CF and T-CF. Digital photos and water droplet contact angle test of (a) the U-CF and (b) T-CF. XPS deconvolution spectra of (c) C1s U-CF, (d) C1s T-CF, (e) O1s U-CF, and (f) O1s U-CF.

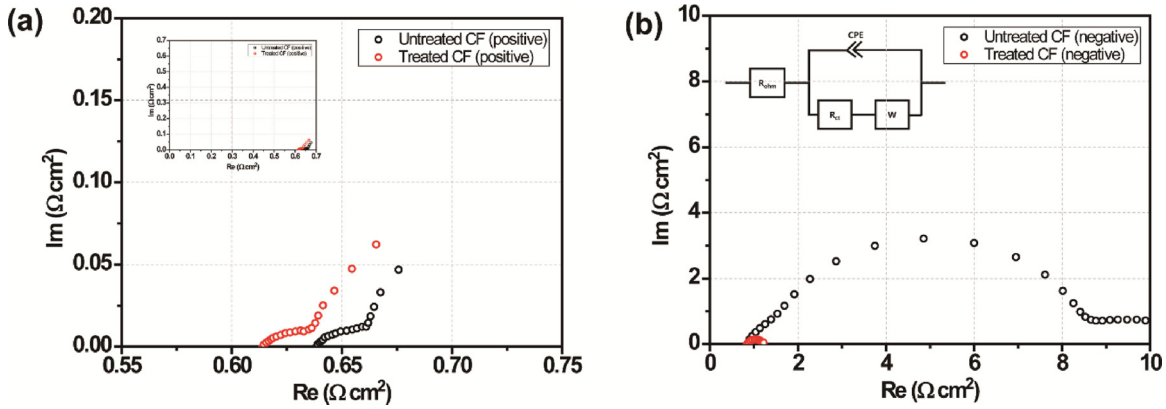


**Fig. 2.** Nyquist plots of the impedances of (a) the $VO_2^+/VO^{2+}$ symmetric cells and (b) $V^{2+}/V^{3+}$ symmetric cells measured at OCV (SOC of 50%). (Electrolyte : 1.5 M $V^{4.5+ \text{ or } 2.5+}$ in 3 M $H_2SO_4$, electrode : the U-CF or T-CF, membrane: NRE 115).

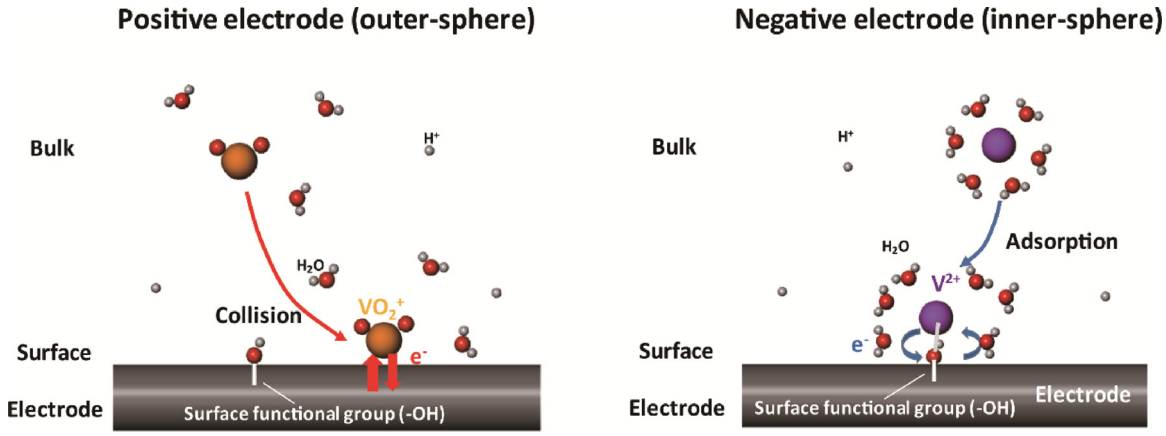


**Scheme 1.** Scheme of outer and inner-sphere mechanism.

(Fig. 1(c) and (d)) and a O1s (Fig. 1(e) and (f)) XPS analysis. As shown in the C1s spectra, the U-CF exhibited the characteristic peaks from C═C (284.6 eV) and C−C (284.7 eV), whereas the T-CF showed an additional peak from −COH (286.6 eV), indicating −OH functionalization. The O1s spectra also indicated that the C═O (or C−O−C) (531.7 eV) and C−O peak (533.3 eV) for the T-CF are much larger than those for the U-CF due to the heat treatment. The survey scan shows that the oxygen content of T-CF was 7.8% and that of U-CF 2.5%.

To investigate the effect of the surface functionalization on the PE and NE, two kinds of symmetric cells were prepared; one employs U-CF for both electrode compartments and the other T-CF. The PE was investigated by flowing 0.75 M $VO^{2+}$/0.75 M $VO_2^+$ with 4.5 M sulfate through the symmetric cells and the NE reaction is studied by flowing 0.75 M $V^{2+}$/0.75 M $V^{3+}$ with 4.5 M sulfate. Fig. 2(a) and (b) show the Nyquist plots of the two positive cells and the two negative cells at an OCV condition (SOC of 50%), respectively. In each case, the symmetric

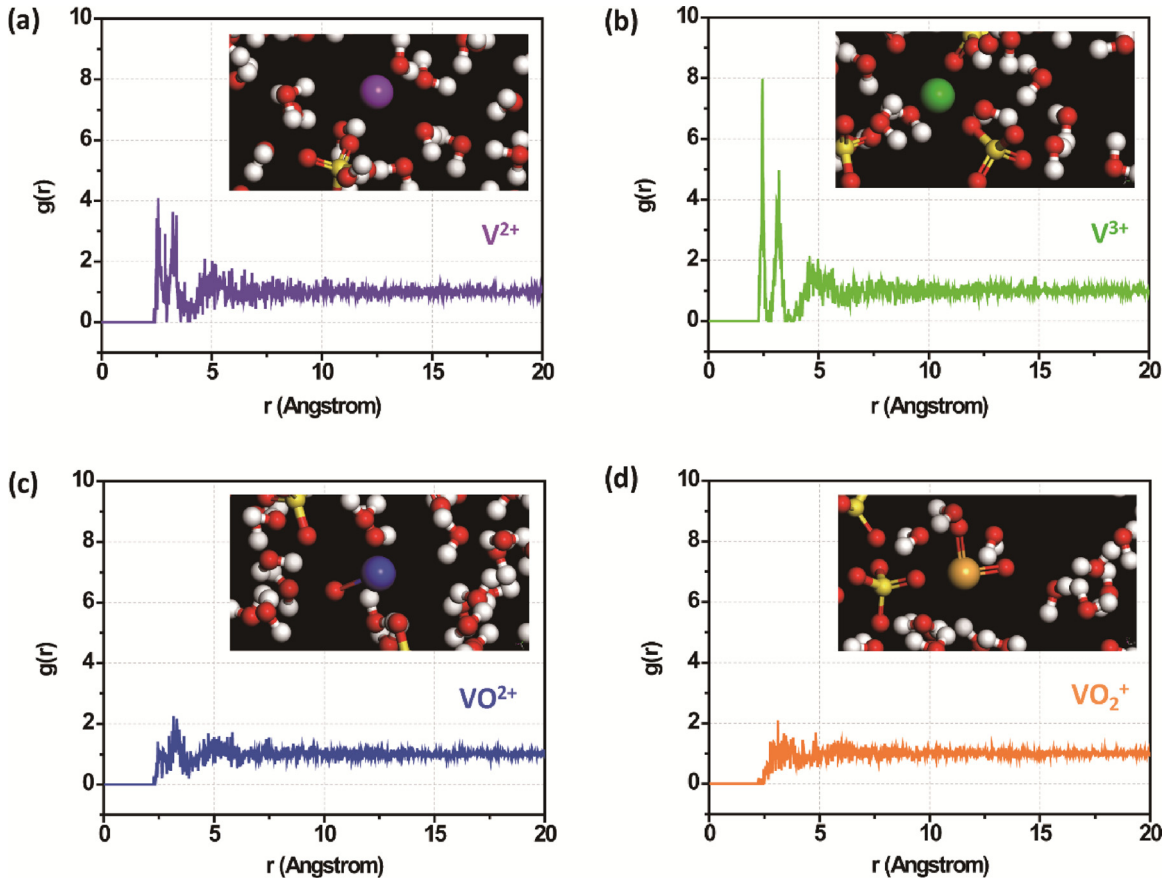


**Fig. 3.** The plot of radial distribution functions between (a) $V^{2+}$, (b) $V^{3+}$, (c) $VO^{2+}$ and (d) $VO_2{}^+$ and $H_2O$ molecules. The inset is a snapshot of the vanadium ions in $H_2SO_4$ solutions after MD simulation with various vanadium oxidation states.

cell with the U-CF and that with the T-CF were compared. Before measuring the impedance of the positive and negative symmetric cells, all electrolytes were circulated for 12 h to ensure sufficient electrolyte infiltration into the U-CF or T-CF in a cell. As shown in Fig. 2(a), the impedances of the positive symmetric cells feature a depressed semi-circle and low frequency tail, which can be assigned to a charge transfer reaction at the electrolyte/electrode interface and semi-infinite diffusion in the boundary layer from the interface. The value for the charge transfer resistance ($R_{ct}$) determined from fitting with the circuit model (inset of Fig. 2(b)) was 0.025 and 0.018 $\Omega$ $cm^2$ for the U-CF and T-CF, respectively. The exchange current densities of the electrodes were also calculated from $R_{ct}$ by using Eq. (3) and are listed in Table S2.

$$i_o = \frac{RT}{FR_{ct}} \tag{3}$$

This indicates that the heat-treatment does not have a notable influence on PE reaction in spite of the large surface structural change. On the other hand, the effect of the heat treatment on the NE reaction was significant as displayed in Fig. 2(b). The negative symmetric cell with the T-CF exhibited a much smaller semi-circle compared with that with the U-CF. The circuit model fitting resulted in a $R_{ct}$ value of 0.159 $\Omega$ $cm^2$ for the T-CF and 3.75 $\Omega$ $cm^2$ for the U-CF. Therefore, the heat treatment effect was vastly stronger in the NE reaction (23.6 times) than in the PE reaction (1.4 times).

The $R_{ct}$ values of the PE reaction were much smaller than those of the NE reaction regardless of the type of CF, indicating a faster kinetics of the PE reaction. This is in good agreement with previous results showing smaller polarizations for the positive half cells [15–18]. In contrast to the perception that the PE reaction is slower due to the additional oxygen transfer step [3,5,6], the symmetric cell results clearly demonstrate the fast kinetics of the PE reaction. The appearance of the low frequency tail for the PE reaction suggests that the diffusion of $VO_2{}^+$ and $VO^{2+}$ ions is important in the reaction rate because of its fast kinetics [15].

The weak dependency on surface functionalization and the relatively small $R_{ct}$ values for the positive symmetric cells collectively suggest that the PE reaction follows an outer-sphere mechanism (Scheme 1). The main feature of outer-sphere electron transfer is that electron transfer between the carbon surface and $VO^{2+}/VO_2{}^+$ ions and oxygen transfer between $VO^{2+}$ and $VO_2{}^+$ ions are possible in the absence of surface adsorption of $VO^{2+}/VO_2{}^+$ ions. In this case, molecule collisions between the electrode and the reactant are the major driver for the electron transfer, and reorganization of the solvation structure of reactant is not necessary. For these reasons, the reaction rate of the PE reaction can be high as Stimming and coworkers previously suggested [18].

On the other hand, the strong dependency on surface functionalization and the relatively large $R_{ct}$ values for the negative symmetric cells suggest that the NE reaction follows an inner-sphere mechanism, as shown in Scheme 1. In the case of inner-sphere electron transfer, the adsorption of the reactant on a specific site on the electrode is critical in accelerating the electron transfer, which corresponds to the model suggested by Kazacos and coworkers [3,5,6]. The adsorption and desorption process that accompanies the rearrangement of a solvated structure imposes a large activation energy for the inner-sphere electron transfer, resulting in a larger $R_{ct}$ value compared to the outer-sphere electron transfer.

Considering the higher charge density of $V^{2+}$ and $V^{3+}$ compared with $VO^{2+}$ and $VO_2{}^+$, it is quite feasible that water molecules are more strongly coordinated to $V^{2+}$ and $V^{3+}$ than to $VO_2{}^+$ and $VO^{2+}$. An atomistic molecular dynamics simulation was performed to identify the hydration structure of the four vanadium ions with different oxidation

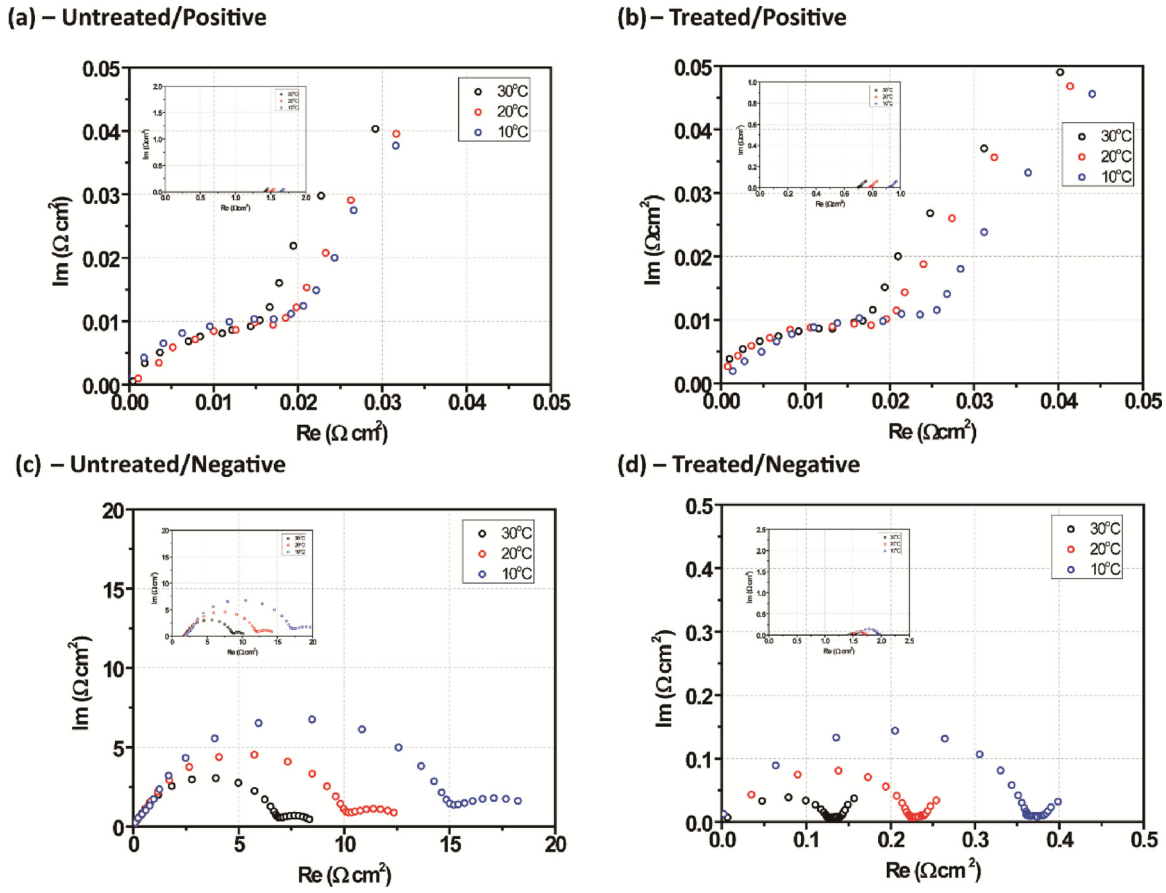


**Fig. 4.** $R_{ohm}$-corrected Nyquist plots of temperature dependent impedances of the positive symmetric cells with (a) U-CF and (b) T-CF, and negative symmetric cells with (c) U-CF and (d) T-CF. In these plots, the real components of the impedances are subtracted by the values for $R_{ohm}$ for an easier comparison of the impedances from the electrode reaction. Inset are the uncorrected, original Nyquist plots. 1.5 M $V^{2.5+}$ or $V^{4.5+}$ vanadium electrolytes were used for the measurements.

states (Fig. 3). Snapshots of the vanadium ions in sulfuric acid solution show that water molecules preferentially surround the vanadium ions due to ion-dipole interaction, forming a hydration shell. From the equilibrium trajectory of the MD simulation, the radial distribution function (RDF) between a vanadium ion and water molecule was calculated.

For $V^{2+}$ and $V^{3+}$, two sharp peaks that correspond to the primary water molecules having a strong interaction with the vanadium ions are clearly shown (Fig. 3(a) and (b)). The one sharp peak centered at 2.4 Å is from V-O ($H_2O$), and the other sharp peak at 3.3 Å is from V-H ($H_2O$) (Fig. S1). The broad peaks (4.8 ~ 5 Å) shown at a longer distance represent the secondary water molecules with a weaker interaction with the vanadium ions. For $VO^{2+}$ ions, the peaks from the primary water molecules are not as apparent as those for the $V^{2+}$ and $V^{3+}$ ions (Fig. 3(c)), indicating a weaker interaction between the $VO^{2+}$ ions and water molecules. $VO_2^+$ ions showed the weakest ordering of the primary water molecules (Fig. 3(d)), as expected from the large ion size and smaller charge number. Since the vanadium ions can be surrounded not by sulfate anion but also bisulfate anion, the MD simulation was repeated with bisulfate anion for $V^{2+}$ and $VO_2^+$. As shown in Fig. S2, $VO_2^+$ ions showed a weaker water coordination than $V^{2+}$, which is in good agreement with the simulation results with sulfate anion.

The simulation provides a feasible explanation for the difference in reaction mechanism for the positive and negative redox reaction. The RDF results suggest that $V^{2+}$ and $V^{3+}$ ion are surrounded by a hard hydration shell due to the strong ion-dipole interaction, whereas $VO^{2+}$ and $VO_2^+$ have a less-organized hydration shell. Since the hydration shell functions as a barrier for electron transfer between CF and vanadium ion, direct electron transfer through the hard hydration shell would be not facile for $V^{2+}$ and $V^{3+}$. Therefore, the OH functional group which helps the breakage of the hydration shell and anchors these vanadium ions on the electrode surface is essential to lower the activation energy for electron transfer. By contrast, for $VO^{2+}$ and $VO_2^+$, direct contact of the vanadium ions and electrode surface is possible during the collision due to the less-organized nature of the hydration shell, enabling electron transfer without the aid of the OH functional group.

The temperature dependency of the PE and NE reactions was also investigated for the symmetric cells with varying operation temperature. To avoid the precipitation of $VO_2^+$ and any side reaction between the functionalized CF and vanadium electrolyte, an upper temperature limit of 30 °C was imposed for the test. Furthermore, due the lowered solubility and increased viscosity of the electrolytes below 0 °C, the temperature was varied as 10, 20 and 30 °C in this analysis. Because the impedance measurements were conducted with flowing to realize a real operation conditions, the increased viscosity at low temperatures lowers reliability. The symmetric cells were immersed in a temperature-controlled bath and the AC impedances were measured under an OCV condition at a SOC of 50%. As displayed in Fig. 4, with an increase of the temperature from 10 to 30 °C, $R_{ohm}$ and $R_{ct}$ decreased for both the positive and negative symmetric cells. The decrease of $R_{ohm}$ can be simply understood by increased ionic conductivity of the electrolytes with temperature [27]. For the PE reaction, the U-CF and T-CF did not show any meaningful difference in the temperature dependency of $R_{ct}$. This can also be ascribed to adsorption of $VO^{2+}/VO_2^+$ ions on the surface functional group not contributing to the redox reaction kinetics due to the fast outer-sphere electron transfer. The temperature dependencies of the NE reaction were stronger than those of the PE both

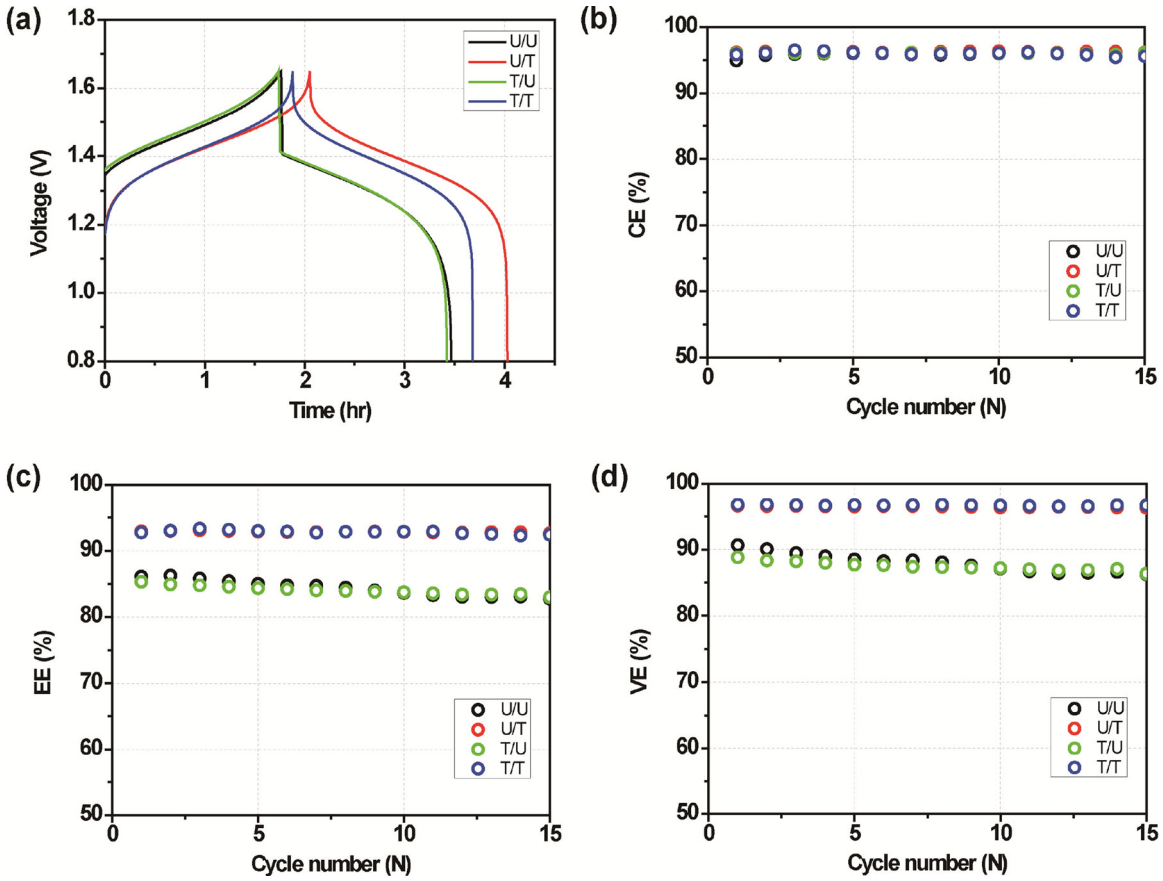


**Fig. 5.** (a) Charge-discharge profiles at 15th cycle, (b) coulombic, (c) energy, (d) voltage efficiencies of the full cell with U/U, U/T, T/U, T/T (current density: 20 $mAcm^{-2}$, flow rate: 40 $mlmin^{-1}$).

for the U-CF and T-CF, indicating larger activation energies for electron transfer. A more detailed description of the activation energies is given in Supporting information (Fig. S3).

Finally, we conducted a performance analysis for the four full cells with alternating use of U-CF and T-CF for PE and NE (U/U: U-CF for PE and NE, T/T: T-CF for PE and NE, U/T: U-CF for PE and T-CF for NE, T/U: T-CF for PE and U-CF for NE). Since the same cell hardware and CFs were used for the symmetric cell and full cell analysis, it is possible to investigate whether the features of the PE and NE observed for the symmetric cell are reflected in full cell performance. Fig. 5(a) compares the cycle charge and discharge curves at the 15th cycle for the four full cells. The U/U and T/U cells showed larger charge and discharge polarizations, whereas the T/T and U/T cells showed smaller charge and discharge polarizations.[1] The surface functionalization of the positive CF electrode did not cause significant differences in cell polarization, whereas the surface functionalization of the negative CF electrode considerably reduces the polarizations regardless of the types of positive CF. The results demonstrate that the surface functionalization does not reduce PE polarization, but it considerably lowers the NE polarization, as expected from the symmetric cell analysis. The charge and discharge capacities were smaller for the cells with the U-CF NE because the charging cell voltages reached the cut-off voltage of 1.65 V at smaller charge capacities.

The coulombic, energy, and voltage efficiencies for the four cells during the first 15 cycles are compared in Fig. 5(b)–(d) respectively. The coulombic efficiencies of these cells were quite similar at around 95%, which is reasonable considering the use of an identical membrane. The voltage efficiency was mainly dependent on the surface functionalization of the NE; the U-CF and T-CF NE showed about a 10% difference in energy and voltage efficiency, respectively. The surface functionalization of the PE did not cause a notable difference in voltage efficiency. The full cell results also dictate the symmetric cell results.

This study provides some insights into the electrode reaction mechanisms and further direction of material or system design for enhancing the performance of VRFBs. (1) The development of NE material is more important than that of PE material in terms of enhancing voltage and energy efficiencies. (2) Molecular scale understanding of the structural rearrangement of the solvated vanadium ions for the inner-sphere electron transfer would be critical for an advanced electrode and electrolyte design. (3) For PE, increasing the electrode surface area, electrolyte wetting, and mass transport would be effective in enhancing the kinetics, whereas for NE, structural and compositional designs of active functional groups that can help the adsorption of $V^{2+}$ and $V^{3+}$ ion are critical.

## 4. Conclusion

In order to identify the controversial mechanisms of PE and NE reactions in VRFBs, an impedance analysis was conducted for positive and negative symmetric cells. U and T-CF were compared for the symmetric cells. The PE reaction is weakly sensitive to the CF treatment, whereas the NE reaction is significantly accelerated by the CF treatment. Also, the charge transfer resistances of the PE reaction were much smaller than those of the NE reaction regardless of the CF treatment. These results collectively indicate that the positive electrode reaction does not rely on the surface adsorption, following an outer-sphere mechanism, whereas the negative electrode reaction can be

[1] The difference in the charge/discharge curve between U/T (red) and T/T (blue) (Fig. 5a) is due to not a polarization difference but a difference in electrolyte capacity.

described by an inner-sphere mechanism, which accompanies the adsorption of the reactant. A MD simulation of the hydrated structures of the vanadium ions suggests that the structure of the hydration shell is harder for $V^{2+}$ and $V^{3+}$ compared with $VO^{2+}$ and $VO_2^{+}$, which provides a feasible explanation for the different mechanisms. The comparison of the activation energies further supports the mechanisms. The features of the electrode reactions observed for the symmetric cells were reflected in full cell performance. The improved understanding of the positive and negative redox reaction will be helpful in determining a rational design of electrodes and electrolyte materials.

## Acknowledgements

This work was supported by the Korea Institute of Energy Technology Evaluation and Planning (KETEP) and the Ministry of Trade, Industry & Energy (MOTIE) of the Republic of Korea (No. 20172420108480). This research also has been performed as a co-operation project of “Enhancing durability of redox flow batteries” and supported by the Korea Research Institute of Chemical Technology (KRICT).

## Appendix A. Supplementary data

Supplementary material related to this article can be found, in the online version, at doi:https://doi.org/10.1016/j.est.2018.11.002.

## References

[1] A.Z. Weber, M.M. Mench, J.P. Meyers, P.N. Ross, J.T. Gostick, Q.H. Liu, J. Appl. Electrochem. 41 (2011) 1137–1164.
[2] C. Choi, S. Kim, R. Kim, Y. Choi, S. Kim, H.Y. Jung, J.H. Yang, H.T. Kim, Renew. Sustain. Energy Rev. 69 (2017) 263–274.
[3] M. Rychcik, M. Skyllas-Kazacos, J. Power Sources 22 (1988) 59–67.
[4] L.Y. Li, S. Kim, W. Wang, M. Vijayakumar, Z.M. Nie, B.W. Chen, J.L. Zhang, G.G. Xia, J.Z. Hu, G. Graff, J. Liu, Z.G. Yang, Adv. Energy Mater. 1 (2011) 394–400.
[5] K.J. Kim, M.S. Park, Y.J. Kim, J.H. Kim, S.X. Dou, M. Skyllas-Kazacos, J. Mater. Chem. A 3 (2015) 16913–16933.
[6] B. Sun, M. Skyllas-Kazacos, Electrochim. Acta 37 (1992) 1253–1260.
[7] L. Cao, M. Skyllas-Kazacos, D.-W. Wang, J. Electrochem. Soc. 163 (2016) A1164–A1174.
[8] M.-A. Goulet, M. Skyllas-Kazacos, E. Kjeang, Carbon 101 (2016) 390–398.
[9] M.Y. Liu, Z.P. Xiang, H.Q. Deng, K. Wan, Q.B. Liu, J.H. Piao, Y.Y. Zheng, Z.X. Liang, J. Electrochem. Soc. 163 (2016) H937–H942.
[10] M.Y. Liu, Z.P. Xiang, J.H. Piao, J.Y. Shi, Z.X. Liang, Electrochim. Acta 259 (2018) 687–693.
[11] C. Fabjan, J. Garche, B. Harrer, L. Jörissen, C. Kolbeck, F. Philippi, G. Tomazic, F. Wagner, Electrochim. Acta 47 (2001) 825–831.
[12] X.W. Wu, T. Yamamura, S. Ohta, Q.X. Zhang, F.C. Lv, C.M. Liu, K. Shirasaki, I. Satoh, T. Shikama, D. Lu, J. Appl. Electrochem. 41 (2011) 1183.
[13] L. Yue, W. Li, F. Sun, L. Zhao, L. Xing, Carbon 48 (2010) 3079–3090.
[14] E. Ventosa, M. Skoumal, F.J. Vazquez, C. Flox, J.R. Morante, J. Power Sources 271 (2014) 556–560.
[15] C. Choi, Y. Choi, S. Kim, H.-y. Jung, H.-T. Kim, Electrochim. Acta 213 (2016) 490–495.
[16] D.S. Aaron, Z. Tang, J.S. Lawton, A.P. Papandrew, T.A. Zawodzinski, ECS Trans. 41 (2012) 43–51.
[17] D. Aaron, C.N. Sun, M. Bright, A.B. Papandrew, M.M. Mench, T.A. Zawodzinski, ECS Electrochem. Lett. 2 (2013) A29–A31.
[18] H. Fink, J. Friedl, U. Stimming, J. Phys. Chem. C 120 (2016) 15893–15901.
[19] M. Cecchetti, A. Casalegno, M. Zago, J. Power Sources 400 (2018) 218–224.
[20] B. Sun, M. Skyllas-Kazacos, Electrochim. Acta 37 (1992) 2459–2465.
[21] T. Yamamura, N. Watanabe, T. Yano, Y. Shiokawa, J. Electrochem. Soc. 152 (2005) A830–A836.
[22] M.-y. Liu, Z.-p. Xiang, H.-q. Deng, K. Wan, Q.-b. Liu, J.-h. Piao, Y.-y. Zheng, Z.-x. Liang, J. Electrochem. Soc. 163 (2016) H937–H942.
[23] I. Derr, M. Bruns, J. Langner, A. Fetyan, J. Melke, C. Roth, J. Power Sources 325 (2016) 351–359.
[24] E. Sum, M. Rychcik, M. Skyllas-Kazacos, J. Power Sources 16 (1985) 85–95.
[25] E. Sum, M. Skyllas-Kazacos, J. Power Sources 15 (1985) 179–190.
[26] A. Bourke, N. Quill, R.P. Lynch, D.N. Buckley, ECS Trans. 61 (2014) 15–26.
[27] S.B. Xiao, L.H. Yu, L.T. Wu, L. Liu, X.P. Qiu, J.Y. Xi, Electrochim. Acta 187 (2016) 525–534.